

II. RELATED WORK

Target tracking is the process of recursively the dynamic states of one or more moving objects using sensor measurements. As a critical component of autonomous driving systems, it can be broadly classified into Multi-Target Tracking (MTT) and Extended Target Tracking (ETT) approaches, and then further divided depending on the sensors used and the vehicle dynamic estimator and model employed.

MTT algorithms maintain separate tracks, one for each object, assuming one measurement per object per timestep. Classical MTT frameworks, such as Multiple Hypothesis Tracking (MHT) [1] and Joint Probabilistic Data Association (JPDA) [2], handle data association uncertainties. ETT methods address scenarios where a single extended object generates multiple measurements [3].

For state estimation, the Extended Kalman Filter (EKF) is a popular choice for its computational efficiency and handling of nonlinear measurements [4]. More advanced model-based methods, such as the Unscented Kalman Filter (UKF) and Particle Filters (PF), have been developed for stronger nonlinearities or non-Gaussian distributions [5]. Although computationally intensive, these filters can offer significant accuracy improvements over EKF in challenging scenarios.

The chosen motion model significantly impacts tracking performance for model-based estimators like EKF and UKF. Simple models like constant velocity (CV) and constant acceleration (CA) serve as basic assumptions for target dynamics [6]. However, vehicles often perform complex maneuvers better represented by nonlinear models, such as Constant Turn Rate And Velocity (CTRV) and Constant Turn Rate And Acceleration (CTRA)[7]. Advanced modeling techniques, like the Interacting Multiple Model (IMM) estimator, combine multiple motion models to adapt dynamically to changing vehicle behavior [8], although at the cost of increased computational and implementation effort.

Sensor fusion [9], particularly combining LiDAR and RADAR, leverages complementary sensor strengths to improve tracking robustness and accuracy [10]. LiDAR offers precise spatial positioning, while RADAR provides larger range and direct Doppler range-rate measurements. [11] and [12] demonstrated superior vehicle tracking performance by integrating LiDAR and RADAR data, although they lack the explicit integration of Range Rate Measurements. Fusion frameworks typically manage sensor latency and unsynchronized measurements via buffering and augmented filtering techniques [10].

Despite extensive research, current methods exhibit limitations in high-speed autonomous racing. Existing algorithms often neglect direct integration of RADAR Doppler range-rate measurements into state estimation, limiting velocity estimation accuracy. Additionally, most validations occur in urban or highway scenarios, lacking testing under the high dynamics and speeds of autonomous racing. These gaps underscore the necessity of specialized sensor fusion algorithms designed explicitly for high-speed racing environments.

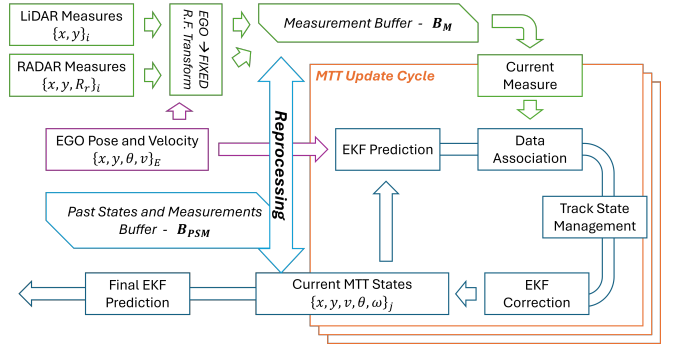


Fig. 2. The proposed algorithm architecture with its main components

III. METHODOLOGIES

In this section, we present our approach for Target Tracking via LiDAR-RADAR sensor fusion for autonomous racing. We developed a Multi Target Tracking (MTT) algorithm using an Extended Kalman Filter (EKF) for track dynamics estimation enhanced with a measurement buffering system that compensates for sensor latency and manages Out-of-Sequence Measurements (OOSM). We model the vehicle dynamics using a Constant Velocity Turn Rate (CVTR) model and introduce a Yaw Rate Exogenous Input to further refine state estimation accuracy. A Finite State Machine (FSM) manages track initialization and termination, while Data Association is handled through a Global Nearest Neighbor (GNN) search.

We propose an algorithm that works under the availability of the following signals:

- A smooth 2D absolute EGO vehicle pose and velocity estimation *e.g.* from an INS/GNSS receiver
- A set of LiDAR object 2D position measurements *e.g.* from a clustering algorithm [13]
- A set of RADAR object 2D positions and Range Rate Measurements

All of the aforementioned signals come from sensors mounted on the moving sensing platform (EGO Vehicle), although the methods can be expanded to use signals coming from external sources like V2V communication. The sensors are supposed to be calibrated w.r.t. a common reference frame fixed on the EGO vehicle. We assume the sensor measurement delay to be known, even if time-varying. If no reliable delay measure is available, an average constant value should be identified experimentally via suitable calibration procedures.

The proposed Target Tracking algorithm structure is shown in Figure 2, and is implemented as a ROS2 node. All the elements composing the algorithm will be explained in more detail within the following subsections.

A. MTT cycle with Variable Time Step

In order to operate online, we implemented the algorithm as a fixed-rate ROS2 node with a *Measurement Buffer* B_M . The main algorithm iterates at a fixed frequency of 33 Hz, higher than the frequency of both sensors. Incoming

measurements between Target Tracking iterations are accumulated in B_M , which is implemented as an Ordered Map with the measurement timestamp t_{meas} as the map key.

At each algorithm iteration, we perform a full *Multi Target Tracking Update Cycle*, composed of *EKF Prediction*, *Data Association*, *Track State Management* and *EKF Correction*, for every measurement in B_M , independently of its kind (LiDAR or RADAR), as from Figure 2. Every measurement is removed from the buffer after its processing, and the next measurement is processed. The iteration ends when the buffer is empty. If the buffer was already empty at the beginning of the iteration, we still perform the Target Tracking cycle, even if only *EKF Prediction* actually takes place, as the other stages aren't defined without new measurements.

After processing a measurement, the MTT timestamp t_{MTT} is updated to the timestamp of the most recent processed measurement, t_{meas}^{old} . If no measurement has been processed in the current iteration, t_{MTT} is incremented by the time elapsed since the last iteration. The time step T used for the EKF model discretization is computed as $T = t_{meas} - t_{MTT}^{old}$, with t_{MTT}^{old} denoting the value of t_{MTT} before processing the current measurement. To compensate for the sensor delay, the output of the MTT algorithm is always subject to a last EKF prediction by a time step equal to $T_{out} = t_{curr} - t_{MTT}$ with t_{curr} being the current time. The EKF state is not changed during this last prediction.

B. Out-of-Sequence Measurements Management

If the measurement delay is large or varies greatly between the sensors, it may happen to have $T < 0$. This is the definition of an Out-of-Sequence Measurement (OOSM), as we need to process a measurement older than the current state estimate.

We implemented a *Reprocessing* strategy to handle OOSMs, which involves the use of an additional buffer, the *Past States and Measurements Buffer* B_{PSM} , again implemented as an Ordered Map. After each MTT cycle update, we add a snapshot of the current Track EKF states and the corresponding input measurements (if any) to B_{PSM} , with $t_{meas} = t_{MTT}$ as the key.

When an OOSM occurs, we traverse B_{PSM} from the last element until we find a states/measurements pair that is older than the OOSM timestamp. In the process, we add all the encountered measurements to B_M . We then roll back the MTT algorithm's state to the snapshot from B_{PSM} that precedes the OOSM, and proceed to process all the measurements added to B_M , including the OOSM that triggered the Reprocessing, following the standard MTT cycle.

C. EKF Update, State and Input

For each tracked target, we instantiate an EKF to estimate its dynamics by filtering the associated measurements. The EKF is composed of a state update function \mathbf{F} and an output function \mathbf{H} according to

$$\begin{aligned} X(k+1) &= \mathbf{F}(X_k, u_k) + Q \\ Y(k) &= \mathbf{H}(X_k) + R \end{aligned} \quad (1)$$

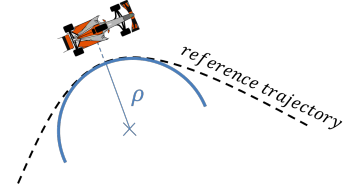


Fig. 3. Computation of the Yaw Rate Exogenous Input

As the EKF state update function \mathbf{F} , we employ a reduced-state version of the Constant Velocity and Turn Rate (CVTR) model in its polar form [7]. This model describes the motion of a kinematic point along a circular path, with constant linear and angular velocity, and it is widely employed in Target Tracking literature. It is described in continuous time form as

$$\dot{\mathbf{X}}(t) = \begin{bmatrix} \dot{x}(t) \\ \dot{y}(t) \\ \dot{v}(t) \\ \dot{\theta}(t) \end{bmatrix} = \begin{bmatrix} v(t) \cos(\theta(t)) \\ v(t) \sin(\theta(t)) \\ 0 \\ \omega(t) \end{bmatrix} \quad (2)$$

where the state vector $\mathbf{X}(t) = [x, y, v, \theta] \in \mathbb{R}^4$ describes the target pose and linear velocity in an inertial, earth-fixed reference frame. The yaw rate ω is defined as an exogenous input $u \in \mathbb{R}$.

The CVTR model allows for the exact discretization, which holds for any time step, enabling us to vary the time-step at runtime to accommodate non-constant sensor sampling rate and delay, as described by

$$\mathbf{X}(k+1) = \begin{bmatrix} x_k + \frac{2v_k}{\omega_k} \sin\left(\frac{\omega_k T}{2}\right) \cos\left(\theta_k + \frac{\omega_k T}{2}\right) & \omega_k \neq 0 \\ x_k + v_k T \cos(\theta_k) & \omega_k = 0 \\ y_k - \frac{2v_k}{\omega_k} \sin\left(\frac{\omega_k T}{2}\right) \sin\left(\theta_k + \frac{\omega_k T}{2}\right) & \omega_k \neq 0 \\ y_k + v_k T \sin(\theta_k) & \omega_k = 0 \\ v_k & \\ \theta_k + \omega_k T & \end{bmatrix} \quad (3)$$

where the Yaw Rate Exogenous Input ω is computed by multiplying the current track velocity estimate $v(k) = X_3$ by the curvature of a reference trajectory parallel to the track centerline. The curvature is computed from the second-order Taylor approximation of the reference trajectory at the point closest to the tracked vehicle pose, as Figure 3 shows, according to:

$$u = \omega = v \cdot \rho_{closest} \quad (4)$$

The rationale behind the use of this Yaw Rate Exogenous Input comes from three observations: the first one is that a vehicle moving on a racetrack close to its performance limit, even when performing racing maneuvers like overtakes, will still have a very small incidence angle w.r.t. the track centerline, as the majority of its lateral (yaw rate) dynamics will be employed to stay within the track bounds. The second observation lies in the difficulty of estimating a state that is not measured directly but instead is the derivative of another state, again not measured directly and with a non-linear

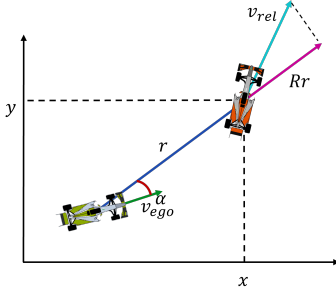


Fig. 4. Representation of the components of the Range Rate measurements: Line-of-Sight angle α , etc...

dependence on the measurements. The third observation lies in its minor role in path planning: during overtaking maneuvers the EGO and opponent vehicles will be in close proximity, and therefore the opponent motion prediction will be mostly based on the opponent position, velocity and heading.

D. EKF Measurement Function

The EKF measurement function $\mathbf{H}(X)$ is time-varying and size-varying, as the shape of the measurement depends on the type of sensor employed: it can be $Y_L = [x, y] \in \mathbb{R}^2$ or $Y_R = [x, y, R_r] \in \mathbb{R}^3$. For both LiDAR and RADAR measurements, we apply the transformation from local (EGO) to global (earth-fixed) reference frame for the x, y position measurements, in order to have them in the same reference frame as the EKF model.

The LiDAR measurement function is linear, as after the reference frame transformation the LiDAR directly measures the first two states, giving $Y(k) = H_L \cdot X(k)$, from which derives:

$$H_L = \begin{bmatrix} 1 & 0 & 0 & 0 \\ 0 & 1 & 0 & 0 \end{bmatrix} \quad (5)$$

The RADAR measurement function instead is non-linear and time-varying as the Range Rate represents the relative EGO-target velocity expressed in the EGO reference frame and projected on the Line-of-Sight defined by the bearing angle α , as Figure 4 shows. Therefore, the RADAR measurement function depends not only from the target states but also on the EGO velocity and heading, which are assumed to be known.

Given the knowledge of the EGO velocity and heading v_E, θ_E , the Range Rate equation is:

$$R_r = [-v \cos(\theta) \sin(\theta_E) + v \sin(\theta) \cos(\theta_E)] \sin(\alpha) + [v \cos(\theta) \cos(\theta_E) + v \sin(\theta) \sin(\theta_E) - v_E] \cos(\alpha) \quad (6)$$

and its corresponding linearized measurement matrix can be derived as:

$$H_R = \begin{bmatrix} 1 & 0 & 0 & 0 \\ 0 & 1 & 0 & 0 \\ 0 & 0 & \frac{dR_r}{dv} & \frac{dR_r}{d\theta} \end{bmatrix} \quad (7)$$

E. EKF Prediction and Data Association

The first step of every MTT cycle is EKF Prediction, in which every track is subject to motion prediction according to Equation (3). The yaw rate input u is computed according to (4) for every track and then used to update the state estimation.

During the prediction step, we apply (1) in order to compute both the predicted state $\hat{X}(k+1)$ and its corresponding predicted output \hat{Y} . We also update the current state and output error covariance estimation according to:

$$\begin{aligned} \hat{X}(k) &= \mathbf{F}(X_{k-1}, u_k) \\ \hat{Y}(k) &= \mathbf{H}(\hat{X}_k) \\ A(k) &= \left. \frac{d\mathbf{F}}{dx} \right|_{\hat{X}_k} \\ P(k) &= A_k P_{k-1} A_k^T + Q \\ S(k) &= H_{L,R} P_k H_{L,R}^T + R \end{aligned} \quad (8)$$

where A represents the state linearization around the current prediction, P the state error covariance estimate and S the output error covariance estimate, while Q and R represent the model and output noise covariance matrices.

We associate the incoming measurements to the predicted track position by computing the Mahalanobis Distance for every track-measurement pair, defined as D_m . To ensure a uniform distance computation across different sensor types, we only employ the $\{x, y\}$ position of the RADAR measurement and the relative submatrix of S according to:

$$\begin{aligned} E_m &= [\hat{x} - x_{meas}, \hat{y} - y_{meas}] \\ D_m &= E_m \cdot (S_{1:2, 1:2})^{-1} \cdot E_m^T \end{aligned} \quad (9)$$

We evaluate the Mahalanobis Distance for every track-measure pair, building a cost matrix. We impose an upper Gating Threshold on the computed Mahalanobis distance in order to inhibit the association of measures that are too far away from the corresponding track, and then we use the Munkres Algorithm to find the track-measurement assignment with the lowest overall cost.

The use of the Mahalanobis distance for data association allows the data association process to encompass information about the current track state estimation confidence: a track that has not been corrected for long will have a larger association region to reflect the larger uncertainty associated to the current vehicle pose estimate.

After the Data Association step, measurements associated to a track will be used to correct the EKF state prediction, while those measurements that have not been associated to an existing track will be used to spawn a new track.

F. Track Management

After the Data Association step, we know which tracks have been associated with a measure in the last iteration and which have not. This information is accumulated and used to enable the transitions of the Track Management Finite State Machine represented in Figure 5.

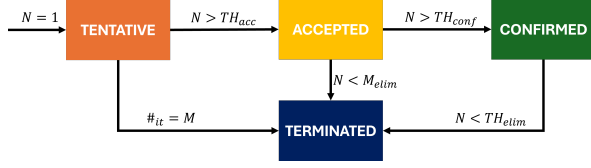


Fig. 5. Track Management Finite State Machine states and transition

For every track, we define a FSM with four states: *Tentative*, *Accepted*, *Confirmed* and *Terminated*. Every track FSM is initialized in the *Tentative* state, with the *Terminated* state being the terminal state, after which the track is deleted. Only *Confirmed* tracks represent the output of the Target Tracking algorithm, while *Accepted* tracks represent an intermediate state.

The state transition function of the FSM depends on the so-called *M/N Logic*, meaning that state transitions are enabled if the corresponding track has received at least N measurements in the last M MTT cycles. We define two upper thresholds, TH_{acc} and $TH_{conf} > TH_{acc}$ for the transition from *Tentative* to *Accepted* and from *Accepted* to *Confirmed* respectively. A lower threshold, $TH_{elim} < TH_{acc}$ is used to transition tracks from either the *Accepted* or *Confirmed* states to the *Terminated* state if not met, effectively eliminating them. The elimination of *Tentative* tracks happens if, once M measurements have been received, the track has not been *Accepted*, to quickly eliminate false positives.

G. EKF Correction

The last step of the MTT cycle is the actual EKF correction, in which we use the measurement associated to every track (except *Terminated* tracks) to correct the estimation of its dynamical state using the EKF Update equations:

$$\begin{aligned} E(k) &= (Y_k - \hat{Y}_k) \\ L(k) &= P_k \cdot H_{L,R}^T(k) \cdot S_k^{-1} \\ X(k) &= X_{k-1} + L \cdot E_k \end{aligned} \quad (10)$$

where E is the measurement error or innovation of associated measurement Y and L is the Kalman Gain.

This EKF correction is not applied to the first associated measurement of a track, which determines the track creation and is initialized with $v = 0, \theta = 0$, nor for the second associated measurement. To speed up the EKF convergence, we perform the Two Step Initialization procedure described in [14]. During this procedure we compute the initialization velocity and heading as:

$$\begin{aligned} v_2 &= \sqrt{(x_2 - x_1)^2 + (y_2 - y_1)^2} \\ \theta_2 &= \arctan((y_2 - y_1)/(x_2 - x_1)) \end{aligned} \quad (11)$$

This procedure quickly initializes the track's velocity and heading to values that, although noisy, enable faster convergence to the true values compared to a default zero initialization.

IV. EXPERIMENTAL RESULTS

The vehicle used for the experimental data collection and algorithm validation is a Dallara AV21 *minerva*. It is a single-seater autonomous race car equipped with three Luminar Hydra LiDAR sensors, positioned in order to have 360° coverage around the vehicle (although with some minor blind spots), and a single forward-facing APTIV ESR 2.5 RADAR sensor. The vehicles are equipped with two NovAtel PwrPak7D RTK INS/GNSS receivers which act both as the EGO vehicle localization source for the algorithm operations as well as a Ground Truth source for performance evaluation.

We evaluate the algorithm performance on two datasets: the first is an experimental dataset taken at the Las Vegas Motor Speedway during the 2023 IAC event. It consists of 15 overtaking maneuvers captured both by the overtaking and overtaken vehicle perspective at speeds ranging from 160 to 275 km/h. Due to the nature of the oval racetrack, as well as the racing regulations which imposed specific speed brackets for the overtaken vehicle, this dataset is characterized by long sequences at almost constant EGO and opponent speed.

To overcome this limitation, we generated the second dataset using the experimental data acquired during the PoliMOVE qualifying lap at the 2023 IAC event at the Autodromo Nazionale di Monza, by simulating a chasing vehicle following a leader using the recorded trajectories of the real vehicle. We added noise to the ideal sensor measurement with a zero-mean Gaussian model, following the noise characterization of the real sensor data w.r.t. the Ground Truth. Figure 6 shows the different acceleration profile of the two datasets, showing the highly variable vehicle speed of the Monza Racetrack.

We evaluate the tracking performance by measuring the absolute difference between the filtered track states and the ground truth data acquired from the RTK GNSS. To distinguish between forward (longitudinal) and lateral offsets, we transform both tracked and ground-truth states into an EGO-centered coordinate system, computing errors in the local x and y . Moreover, we utilize identical EKF parameters and noise covariances for both the real-world LVMS dataset and the simulated Monza dataset. This uniform setup allows us to assess how well the algorithm generalizes to different

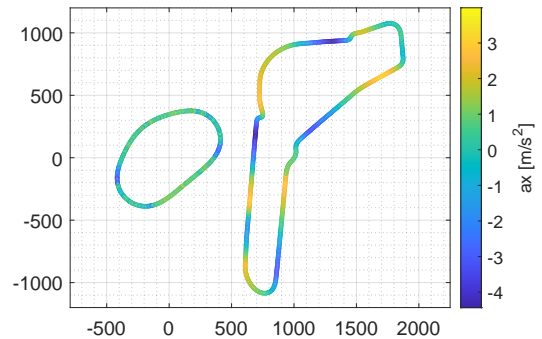


Fig. 6. Map and acceleration profile of the two racing circuits used for this work: on the left, the Las Vegas Motor Speedway, on the right the Autodromo Nazionale di Monza. Distances are expressed in meters.

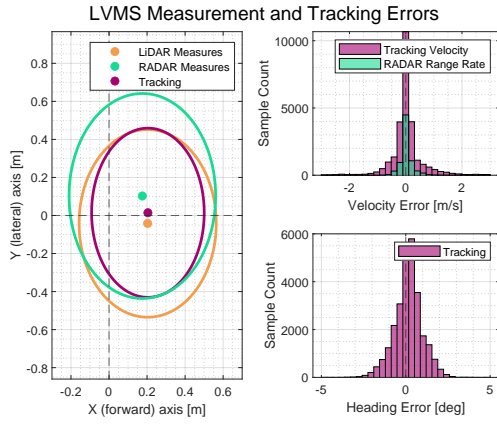


Fig. 7. Experimental measurement and tracking errors w.r.t. the Ground Truth on the LVMS Dataset. On the left, 1-sigma ellipses for the EGO x and y coordinates. On the right, histograms of speed and heading error.

track geometries and acceleration profiles, thus confirming its robustness in diverse racing scenarios.

Figures 7 and 8 show the tracking error of the algorithm on both datasets. We can see that the tracking filter is successfully capable of reducing the estimation error of the measurable states, as well as providing a reasonable estimation of the non-measurable states. The real LVMS data present a bias on the x direction, which derives from sensor mis-calibration, and different mean values between LiDAR and RADAR on the y direction, which are compensated by the EKF. Although in principle the CVTR model is more suited to low acceleration circuits like LVMS, it still manages to provide a consistent tracking and noise reduction on a circuit with a more aggressive longitudinal and lateral acceleration profile. Note that the largest error component is in the lateral direction also on the simulated data, although its acceleration profile was supposed to stress more the longitudinal dynamics estimation.

V. CONCLUSIONS

In this paper, we present a latency-aware EKF-based multi-target tracking framework that integrates LiDAR and RADAR measurements, explicitly incorporating track curvature in the prediction step and RADAR range-rate information in the correction step. By managing Out-Of-Sequence Measurements through state and measurement reprocessing, the proposed can effectively handle the different delays deriving from multi-modal fusion.

Experimental validation on real-world data from the Las Vegas Motor Speedway at speeds up to 275 km/h, as well as a simulated dataset generated from racing laps at the Autodromo Nazionale di Monza, demonstrated robust and reliable estimation performance under widely varying conditions and acceleration profiles.

Future work will extend this approach to include camera-based perception and V2V communication, while also investigating advanced tracking strategies such as Interactive Multiple Models (IMM) to further enhance performance under complex racing maneuvers like heavy braking.

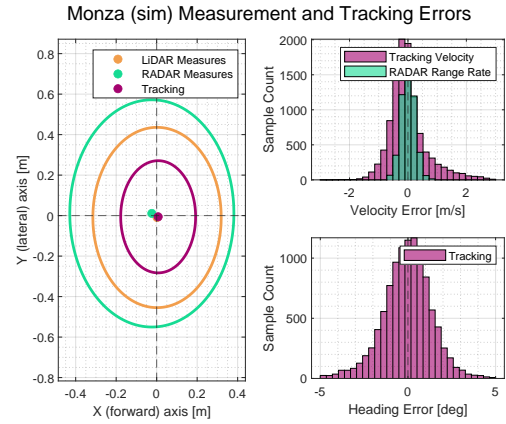


Fig. 8. Experimental measurement and tracking errors w.r.t. the Ground Truth on the Monza simulated dataset. On the left, 1-sigma error ellipses for the local x and y coordinates. On the right, histograms of speed and heading error.

REFERENCES

- [1] E. Dayangac, F. Baumann, J. Aulinas, and M. Zobel, "Target position and speed estimation using lidar," in *Image Analysis and Recognition: 13th International Conference, ICIAR 2016, Póvoa de Varzim, Portugal, July 13-15, 2016, Proceedings 13*. Springer, 2016, pp. 470–477.
- [2] T. Fortmann, Y. Bar-Shalom, and M. Scheffe, "Sonar tracking of multiple targets using joint probabilistic data association," *IEEE Journal of Oceanic Engineering*, vol. 8, no. 3, pp. 173–184, 1983.
- [3] R. Pieroni, M. Corno, F. Parravicini, and S. M. Savaresi, "Design of an automated street crossing management module for a delivery robot," *Control Engineering Practice*, vol. 153, p. 106095, 2024.
- [4] S. J. Julier and J. K. Uhlmann, "Unscented filtering and nonlinear estimation," *Proceedings of the IEEE*, vol. 92, no. 3, pp. 401–422, 2004.
- [5] K. Tian, M. Radovnikovich, and K. Cheok, "Comparing ekf, ukf, and pf performance for autonomous vehicle multi-sensor fusion and tracking in highway scenario," in *2022 IEEE international systems conference (SysCon)*. IEEE, 2022, pp. 1–6.
- [6] X. R. Li and V. P. Jilkov, "Survey of maneuvering target tracking. part i. dynamic models," *IEEE Transactions on aerospace and electronic systems*, vol. 39, no. 4, pp. 1333–1364, 2003.
- [7] M. Roth, G. Hendeby, and F. Gustafsson, "Ekf/ukf maneuvering target tracking using coordinated turn models with polar/cartesian velocity," in *17th International Conference on Information Fusion (FUSION)*. IEEE, 2014, pp. 1–8.
- [8] E. Mazar, A. Averbuch, Y. Bar-Shalom, and J. Dayan, "Interacting multiple model methods in target tracking: a survey," *IEEE Transactions on aerospace and electronic systems*, vol. 34, no. 1, pp. 103–123, 1998.
- [9] D. J. Yeong, G. Velasco-Hernandez, J. Barry, and J. Walsh, "Sensor and sensor fusion technology in autonomous vehicles: A review," *Sensors*, vol. 21, no. 6, p. 2140, 2021.
- [10] B. Khaleghi, A. Khamis, F. O. Karray, and S. N. Razavi, "Multisensor data fusion: A review of the state-of-the-art," *Information fusion*, vol. 14, no. 1, pp. 28–44, 2013.
- [11] H. Lee, H. Chae, and K. Yi, "A geometric model based 2d lidar/radar sensor fusion for tracking surrounding vehicles," *IFAC-PapersOnLine*, vol. 52, no. 8, pp. 130–135, 2019.
- [12] P. Karle, F. Fent, S. Huch, F. Sauerbeck, and M. Lienkamp, "Multi-modal sensor fusion and object tracking for autonomous racing," *IEEE Transactions on Intelligent Vehicles*, vol. 8, no. 7, pp. 3871–3883, 2023.
- [13] M. Cellina, M. Corno, and S. M. Savaresi, "Lidar-based vehicle detection and tracking for autonomous racing," *arXiv preprint arXiv:2501.14502*, 2025.
- [14] Y. Bar-Shalom, X. R. Li, and T. Kirubarajan, *Estimation with applications to tracking and navigation: theory algorithms and software*. John Wiley & Sons, 2004.